Microfluid Nanofluid
DOI 10.1007/s10404-014-1540-6

RESEARCH PAPER

Self-propelled droplets on heated surfaces with angled self-assembled micro/nanostructures

Corey Kruse · Isra Somanas · Troy Anderson · Chris Wilson · Craig Zuhlke · Dennis Alexander · George Gogos · Sidy Ndao

Received: 4 September 2014 / Accepted: 30 December 2014

Abstract Directional and ratchet-like functionalized surfaces can induce liquid transport without the use of an external force. In this paper, we investigate the motion of liquid droplets near the Leidenfrost temperature on functionalized self-assembled asymmetric microstructured surfaces. The surfaces, which have angled microstructures, display unidirectional properties. The surfaces are fabricated on stainless steel through the use of a femtosecond laser-assisted process. Through this process, mound-like microstructures are formed through a combination of material ablation, fluid flow, and material redeposition. In order to achieve the asymmetry of the microstructures, the femtosecond laser is directed at an angle with respect to the sample surface. Two surfaces with microstructures angled at 45° and 10° with respect to the surface normal were fabricated. Droplet experiments were carried out with deionized water and a leveled hot plate to characterize the directional and self-propelling properties of the surfaces. It was found that the droplet motion direction is opposite of that for a surface with conventional ratchet microstructures reported in the literature. The new finding could not be explained by the widely accepted mechanism of asymmetric vapor flow. A new mechanism for a self-propelled droplet on asymmetric three-dimensional self-assembled microstructured surfaces is proposed.

C. Kruse · I. Somanas · G. Gogos · S. Ndao (✉)
Mechanical and Materials Engineering,
University of Nebraska – Lincoln, Lincoln, NE, USA
e-mail: sndao2@unl.edu

C. Kruse
e-mail: coreykruse_08@hotmail.com

T. Anderson · C. Wilson · C. Zuhlke · D. Alexander
Electrical Engineering, University of Nebraska – Lincoln,
Lincoln, NE, USA

Keywords Ratchet · Leidenfrost · Boiling and evaporation · Droplet motion · Directional surfaces · Femtosecond laser

1 Introduction

Controlling and moving liquid droplets are very important in many applications such as microfluidics, ink-jet printing, lab-on-a-chip, and fuel injection for combustion applications. Fluids are conventionally moved through the application of asymmetric potentials such as a pressure gradient (pumps, compressors, etc.) or an electric field (electroosmotic pumps). In microfluidics applications, liquid droplets can be moved and controlled with an asymmetric potential created by varying surface tensions from chemical and thermal gradients (Brochard 1989; Chaudhury and Whitesides 1992; Brzoska et al. 1993; Dos Santos and Ondarcuhu 1995; Darhuber et al. 2003; John et al. 2005) as well as with the use of magnetic fields (Piroird et al. 2012). These methods have the disadvantage of producing very slow droplet velocities (60 μm/s–6 cm/s) as well as typically being limited to a small working distance. An alternative to these methods, which has been recently garnering interest in the scientific community, is self-propelled Leidenfrost droplets on asymmetric surfaces.

A liquid droplet in the Leidenfrost state has the unique characteristic of being supported in a nearly frictionless state by its vapor layer (Linke et al. 2006; Dupeux et al. 2011; Grounds et al. 2012). As a result, it takes very little force to initiate and sustain droplet motion. This characteristic of droplets in the Leidenfrost state has been recently exploited in self-propelled droplets on ratchet surfaces (Linke et al. 2006; Ok et al. 2010; Lagubeau et al. 2011; Dupeux et al. 2011; Marin and del Cerro 2012; Grounds

Published online: 09 January 2015

et al. 2012; Hashmi et al. 2012). Ratchet surfaces have been shown to be very effective at moving liquid droplets over relatively long distances with considerably high speeds, 5–40 cm/s (Linke et al. 2006; Ok et al. 2010; Lagubeau et al. 2011; Dupeux et al. 2011; Marin and del Cerro 2012; Grounds et al. 2012; Hashmi et al. 2012). Recently, tilted micropillars have been shown to also result in Leidenfrost droplet motion (Agapov et al. 2014). Regardless of microstructures arrangement, there has been a general consensus in the literature that the motion of self-propelled Leidenfrost droplets is in the direction opposite to the direction that the microstructures are tilted. It was found recently that the droplet motion directionality can be dependent on the microstructure size and surface temperature (Agapov et al. 2014). Figure 1 shows the Leidenfrost droplet motion directionality corresponding to a conventional ratchet microstructure and the angled self-assembled microstructures used in the present study. As can be seen in the figure, the distinct surfaces result in opposite droplet motion directionality. This paper demonstrates the self-propelled Leidenfrost droplet properties of angled self-assembled metallic micro/nanostructured surfaces formed via femtosecond laser surface processing (FLSP) and sheds light on their opposite directionality compared to conventional ratchet surfaces.

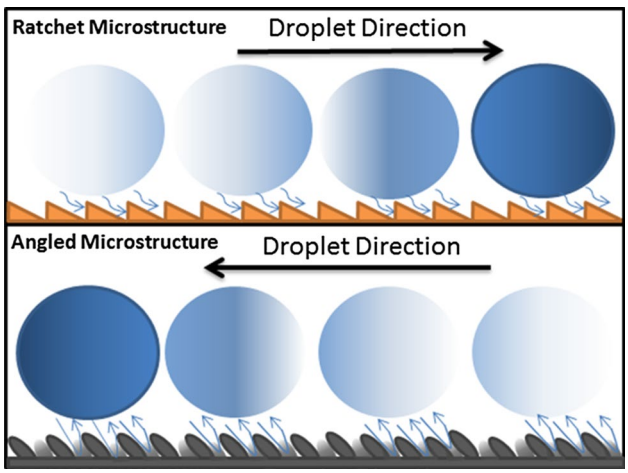

Fig. 1 Schematic describing the droplet motion directionality corresponding to a conventional ratchet surface and the angled FLSP microstructures

2 Experimental procedures

2.1 Sample fabrication

A FLSP technique was used to generate 316 stainless steel surfaces with a quasi-periodic pattern of angled surface microstructures. These surfaces were used to conduct self-propelled Leidenfrost droplet experiments. Surface features (i.e., micro/nanostructures), generated using the FLSP technique, are formed by directly shaping the surface of the bulk material through absorption of energy from multiple femtosecond laser pulses. Absorption of laser energy initiates a complex combination of multiple self-organized growth mechanisms including laser ablation, capillary flow of laser-induced melt layers, and redeposition of ablated material (Nayak et al. 2007; Tsibidis et al. 2013; Zuhlke et al. 2013a, b; Vorobyev and Guo 2013). The size and shape of the features are controlled through fabrication parameters including the laser fluence, the number of laser shots per area incident on the sample, the laser incident angle, and the atmosphere during processing. Furthermore, surface features induced by one laser pulse affect the absorption of light from subsequent pulses, which results in feedback during formation.

A schematic of the FLSP setup is shown in Fig. 2. The fabrication laser was a Ti:sapphire (Spitfire, Spectra Physics) that produced pulses of approximately 50-fs duration with a central wavelength of 800 nm at a 1 kHz repetition rate. The laser power was controlled through a combination of a half-wave plate and a polarizer. The pulses were focused using a 125-mm focal length plano-convex lens (PLCX-25.4-64.4-UV-670-1064) with a broadband antireflection coating covering the laser spectrum. The sample was placed on a computer-controlled 3D translation stage and translated through the beam path of the laser in order to process an area larger than the laser spot size. The number of pulses incident on the sample was controlled by adjusting the translation speed of the sample. The angle of the surface structures was controlled by the incident angle of the laser on the target surface; the surface structures developed with peaks that point in the direction of the incident laser (Hwang and Guo 2011).

In the present study, two stainless steel samples were fabricated with microstructure angles of 45° and 10° with

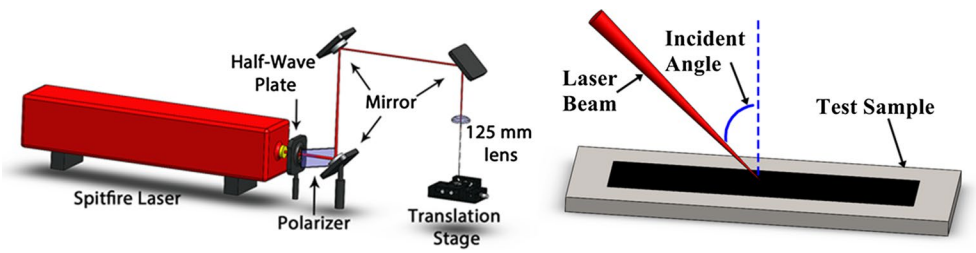

Fig. 2 *Left*—schematic of the femtosecond laser surface processing (FLSP) setup. *Right*—enlarged view of laser beam incident angle

Table 1 Laser parameters and relevant surface characteristics

Structure angle	Pulse energy (μJ)	Number of laser shots	Spot dia. (μm) (parallel)	Spot dia. (μm) (perpendicular)	Peak-to-valley height (μm)	Structure spacing (parallel) (μm)	Structure spacing (perpendicular) (μm)
45	700	500	328	232	17	27	17
10	700	500	188	224	57	29	30

The angle of the microstructures is defined relative to the surface normal. The spot diameters and structure spacing values are defined as parallel or perpendicular to the direction of the laser

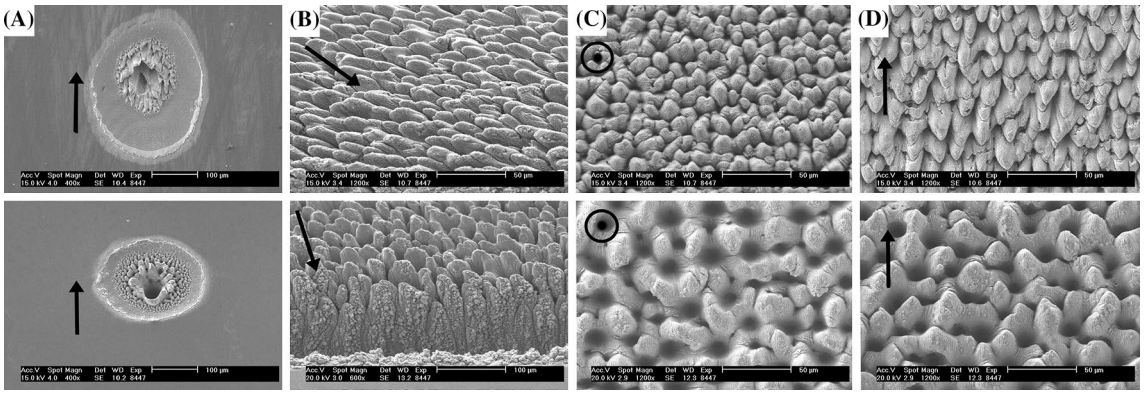

Fig. 3 SEM images of the 45° (*top*) and 10° (*bottom*): **a** laser damage site on the target sample after exposure to 500 laser pulses with a pulse energy of 700 μJ (400× and 100 μm *scale bar*), **b** looking at sides of structures (*top*, 1,200× and 50 μm *scale bar* and *bottom*, 600× and 100 μm *scale bar*), **c** looking along the microstructures (1,200× and 50 μm *scale bar*), and **d** looking normal to the surface (1,200× and 50 μm *scale bar*). The arrows represent the projected direction of the incident laser pulses

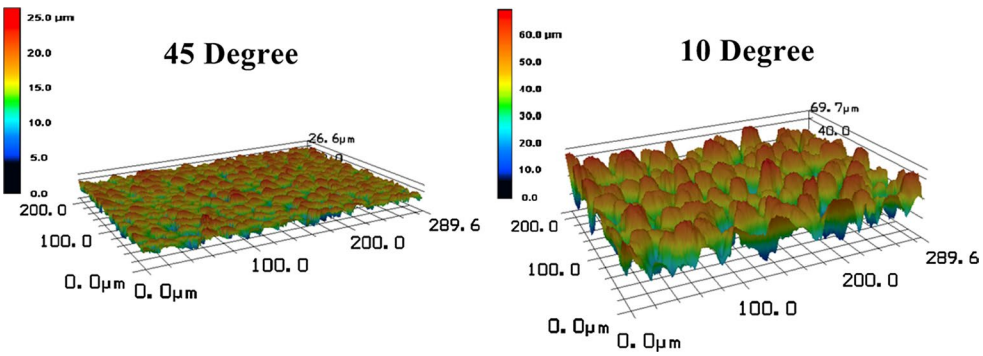

Fig. 4 3D laser confocal images of both the 45° sample and 10° sample

respect to the surface normal and then utilized to demonstrate the ability to self-propel Leidenfrost droplets. These samples are characterized by mound-shaped microstructures that are covered in a layer of nanoparticles and are angled versions of above surface growth (ASG) mound structures (Zuhlke et al. 2013a, b; Kruse et al. 2013). The fabrication parameters as well as relevant surface characteristics are described in Table 1. The two samples were fabricated with the same pulse energy. Because the laser was incident on the sample at an angle, the spot on the sample was elliptical and not the same size for each sample. The elliptical beam profile on the target sample (see Fig. 3a) is due to the non-normal incident angle of the laser. The parallel and perpendicular dimensions given in Table 1 refer to spot size dimensions relative to the laser direction.

Scanning electron microscope (SEM) images of the samples taken from several angles are shown in Fig. 3. The structure spacing values in Table 1 are obtained by a 2D fast Fourier transform (FFT) analysis of the images in Fig. 3c and represent the peak values in the directions parallel and perpendicular to the laser. The peak-to-valley structure heights were measured using a 3D confocal laser scanning profilometer (Keyence, VK-X200); these images are shown in Fig. 4 and correspond to the same surface imaged in Fig. 3. These images were taken at a viewing angle normal to the sample surface. The markedly smaller peak-to-valley

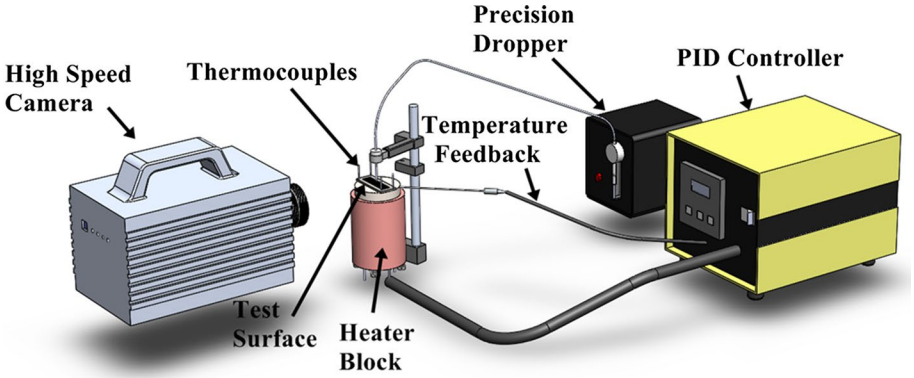

Fig. 5 Schematic of the experimental setup used for characterizing the droplet motion

structure heights of the 45° sample relative to the 10° sample are due to the larger spot size (see Table 1; Fig. 3a) and thus decreased laser fluence on the sample. This relatively lower laser fluence results in decreased surface fluid flow during processing and thus reduced structure development (Zuhlke et al. 2013a).

The two samples were superhydrophilic; this was determined by measuring 0° contact angles with a Ramé–Hart Goniometer. Due to the superwicking nature of the surface, the droplet would perfectly wet the surface and was not able to be directly imaged. The superhydrophilic nature of the surface is a result of the fabrication process (Vorobyev and Guo 2013; Kruse et al. 2013).

2.2 Self-propelled droplet motion experiments

Each of the experimental samples was fabricated on a $2.5'' \times 1''$ piece of polished 316 stainless steel plate. The laser-structured area was $0.5''$ wide and $2''$ long and was located in the center of the plate. Each processed sample was then placed onto a leveled copper heating block heated by five cartridge heaters. Four K-type thermocouples (Omega 5TC-GG-K-36-72) were epoxied (Omega OB-200-2) to the surface of the test sample in order to accurately determine the surface temperature. The surface temperature was monitored with the use of LabVIEW. The surface temperature was controlled through the use of a Ramé–Hart precision temperature controller (Ramé–Hart 100-50) and a thermocouple feedback loop. Droplet size and dispensing was controlled by a Ramé–Hart computer-controlled precision dropper (Ramé–Hart 100-22). Deionized water was used as the working fluid with droplet sizes of 10.5 μL (diameter of 2.8 mm). This size was chosen because it corresponds to the droplet size that easily detaches from the needle by gravity alone. Droplets were released close to the surface to limit the effects of the impact velocity. From high-speed video analysis, using two successive frames immediately before impact, it was determined that the droplets impacted the surface with a velocity of approximately 20 cm/s. This corresponds to a Weber number $\left[\mathrm{We} = \left(\rho D_0 V_0^2\right)/\sigma\right]$ of around 1.5 which is considered to be relatively small ($\rho = 998$ kg/m^3 and $\sigma = 73$ mN/m at room temperature), where ρ is the liquid density, D_0 is the droplet diameter, V_0 is the impact velocity, and σ is the surface tension. All videos were recorded with the use of a high-speed camera (Photron Fastcam SA1.1), set at 250 frames per second. Figure 5 shows a schematic of the experimental setup.

From the high-speed video images, droplet velocities across the samples were calculated using an in-house MATLAB droplet tracking program which tracks the centroid of the droplet. This program calculates the instantaneous horizontal droplet velocity between successive frames and then gives an average velocity profile for the entire droplet motion. The program was validated against droplet velocities manually calculated from still images using a movie editing software; the two methods were in excellent agreement.

3 Results and discussion

Figure 6 shows the data obtained from the droplet motion experiments for the two distinct angled microstructures investigated. Droplets were released onto the surface about $0.5''$ from one processed end, leaving about $1.5''$ of processed length for the droplet to traverse. Velocities presented in Fig. 6 correspond to the maximum droplet velocities at the edge of the processed surface. Each velocity data point corresponds to an average velocity of ten individual droplets, and the error bars correspond to the standard deviation of these ten droplets. As can be seen from the graph, the two curves have similar features yet significant differences. Both curves exhibit a local maximum toward lower surface temperatures. The 45° sample has a maximum velocity of 19.2 cm/s at a surface temperature of 310 °C, while the 10° sample has a maximum velocity of 13.5 cm/s at a surface temperature of 256 °C. For both samples, droplet velocities gradually decrease as the surface temperature is decreased from the maximum observed velocities. At the lowest temperature recorded, both samples displayed a spike in the

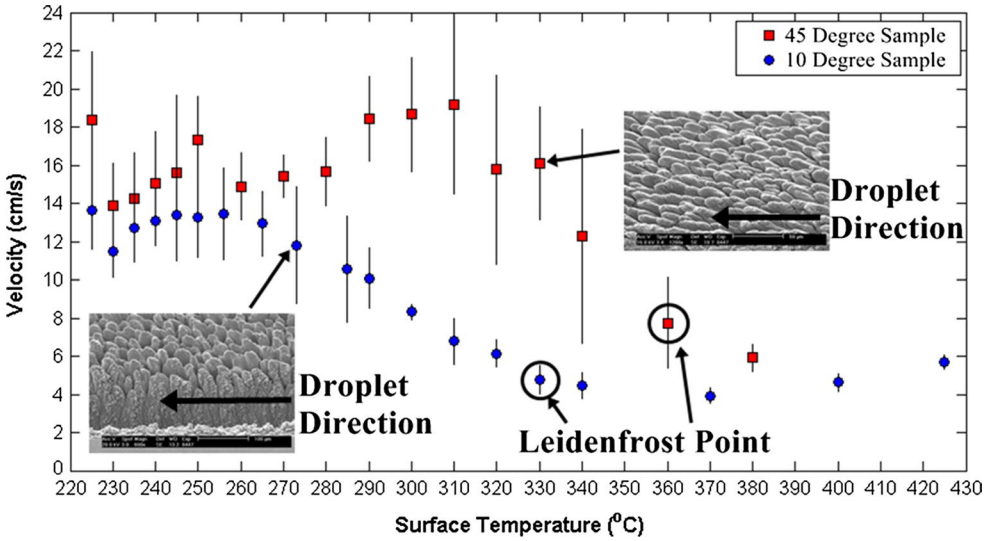

Fig. 6 Droplet velocities with respect to surface temperature for both processed samples

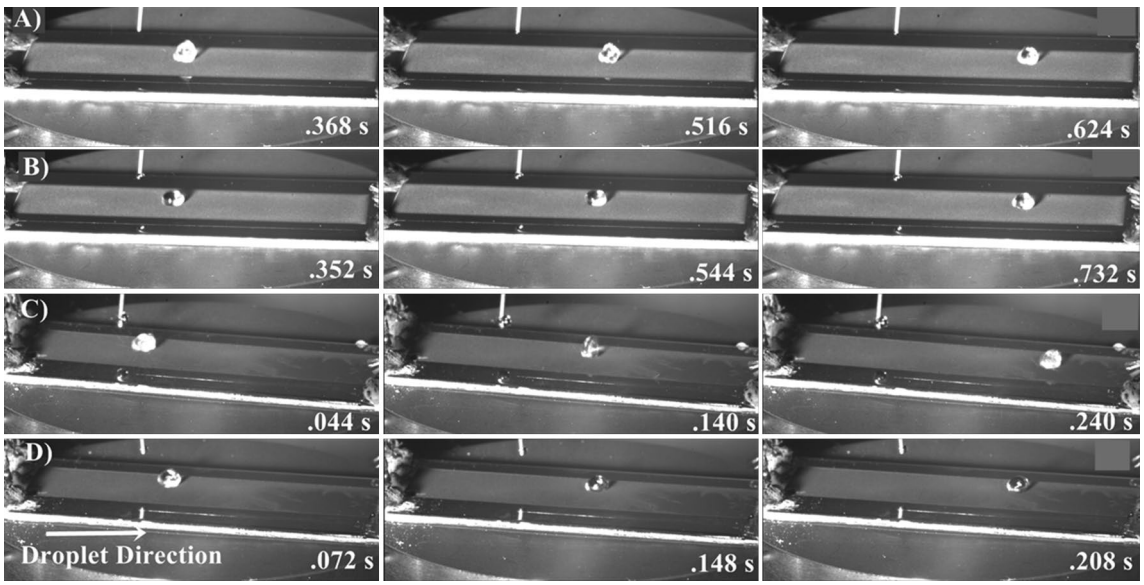

Fig. 7 Droplets at various positions along the leveled sample at temperatures below and at the respective Leidenfrost temperatures with times from initial contact. **a** 10° sample at 320 °C, **b** 10° sample at 330 °C, **c** 45° sample at 340 °C, and **d** 45° sample at 360 °C

droplet velocity. In the case of the 10° sample, this spike in velocity was nearly the same as the local maximum found at 256 °C. Velocities could not be recorded below 225 °C as violent nucleate boiling resulted in the destruction of the liquid droplets. Although the droplet velocities were relatively high at the lowest temperatures, the motion is relatively unstable due to the possibility of nucleate boiling and is thus undesirable for most applications. As the surface temperature is increased beyond the value at the maximum droplet velocity, droplet velocities again decrease but at a much faster rate, especially for the 45° sample.

From Fig. 6, it can be seen that there are two regions of interest. These regions of interest correspond to temperatures above and below the Leidenfrost temperature of the surface. The Leidenfrost temperatures for the 10° and 45° sample were estimated to be 330 and 360 °C, respectively. The Leidenfrost temperature of each surface was estimated by the change in the slope of the curves and the standard deviations of the velocities (Fig. 6) as well as the visual differences in the droplet behavior, captured with the high-speed video images (Fig. 7). Looking at Fig. 6, the slope of the curves changes at 330 and 360 °C for the 10° and 45° samples, respectively. To the left of these temperatures, the standard deviations are significantly larger. This indicates that intermittent contact (Bradfield 1966; Kim et al. 2011; Dupeux et al. 2011; Kruse et al. 2013)

is occurring and the droplet is not in a stable film boiling state. Because this intermittent contact promotes an explosive type of energy transfer, it results in a wide range of droplet velocities and thus larger standard deviations. Figure 7 shows droplets at different locations for temperatures near the Leidenfrost transition temperature for both samples. It can be seen from these images that there is a distinct visual difference in the images of the droplets between the two temperatures. For both samples, the droplets appear to be white in color and not very spherical at temperatures below the Leidenfrost temperature. This indicates that the droplets are being disturbed by intermittent contact. At these temperatures, it can also be seen from the high-speed video that the droplets tend to jump and bounce much more frequently and eject smaller satellite drops. This is characteristic of not having a fully developed vapor film between the droplets and the heated surface and thus below the Leidenfrost region. Flow/thermal instabilities lead to the non-spherical shapes and ejection of satellite droplets. At temperatures at or above the Leidenfrost temperature, the droplets appear to be very spherical and clear in color. This is due to the stable vapor film below the droplet. The Leidenfrost temperatures estimated by this technique are within the expected range for surfaces created by a femtosecond laser process (Kruse et al. 2013). The variation in the Leidenfrost temperature is due to the differences in the surface microstructures (Kruse et al. 2013).

It can be seen from the graph (Fig. 6) and the high-speed images (Fig. 7) that there are two distinctly different mechanisms that aid to the motion of the droplet. The dynamic balance between these two mechanisms results in the characteristics of the velocity curves shown in Fig. 6. At temperatures below the Leidenfrost temperature, droplet motion results from the directional ejection of vapor due to intermittent contact between the liquid droplet and microstructures (Bradfield 1966; Kim et al. 2011; Dupeux et al. 2011; Kruse et al. 2013). When this intermittent contact happens, heterogeneous boiling occurs and vapor is violently released from the droplet resulting in higher droplet velocities. This heterogeneous boiling is likely the cause of the velocity spikes for both samples at 225 °C. At these lower temperatures, contact is more likely to happen and energy is more easily transferred to the droplet. At temperatures above the Leidenfrost temperature, a stable vapor film is created and thus intermittent contact between the droplet and microstructures is less likely to happen. At these temperatures, the droplet motion mechanism is dominated by viscous stresses that drag the droplet in the direction of the vapor flow. Because this mechanism is not abrupt like in the case of intermittent contact, it produces a smaller but more stable force on the droplet and consequently slower velocities. The local maximums for both samples are most likely due to an optimal combination of these two mechanisms.

The overall larger velocities of the 45° sample relative to the 10° sample can be attributed to the difference in microstructure angle between the two samples. The 45° angle results in a more favorable horizontal force component on the droplet during intermittent contact at lower temperatures. The differences at higher temperatures can be explained by a combination of the microstructure size and the viscous drag mechanism. For the 10° sample, the droplet velocity decreases very rapidly with increasing temperatures to reach what seems to be a local velocity plateau (e.g., 370 °C). At temperatures higher than 370 °C in the case of the 10° sample, droplet velocities increase with increasing temperatures due to the increased heat flux to the droplet and a corresponding higher vapor flow velocity. A similar trend was also reported in the literature (Ok et al. 2010) with ratchet structures. No velocities were recorded for the 45° sample above 380 °C because the droplet no longer displayed a preferential directionality. In these temperature ranges, there is little to no intermittent contact and the dominant mechanism is the viscous drag mechanism. The 45° sample has microstructure heights significantly smaller than the 10° sample (see Table 1). This difference in height is the main reason for the different trends at higher temperatures and the lack of directionality for the 45° sample. The viscous drag mechanism is an interaction between the vapor flow, the microstructure geometry, and the droplet base. At high temperatures, the vapor layer is fully developed and relatively thick. In the case of the 45° sample, it is likely that the vapor layer is thick enough to effectively isolate the droplet from the surface microstructures and therefore inhibiting interaction between droplet and surface microstructures, hence no self-propelled motion. Since the 10° sample has significantly taller microstructures (see Table 1), this interaction remains intact at high temperatures and thus the propulsion still occurs.

It was also found that the likelihood of a droplet successfully traveling in the desired direction was highly dependent on the surface temperature. Surface temperatures in the range of 250–360 °C resulted in nearly a 100 % success rate, meaning that a droplet placed on the surface in this temperature range would remain on the processed area and travel the complete length. At temperatures below this range, the success rate decreased quite rapidly due to droplets exploding or boiling when coming into contact with the surface. At higher temperatures, the success rate, once again, also decreased to around 50 %. At these higher temperatures, the droplet was very sensitive to the transition from the needle to the surface. With a stable vapor layer at these high temperatures and a nearly frictionless state, it was observed that if the droplet had any undesirable momentum from the release, it was more likely to travel in an undesirable direction. Because the force acting on the droplet at these high temperatures is fairly small, it is much more difficult to correct the initial droplet direction.

4 Self-propulsion mechanism

Unlike previously published studies in the literature, the direction of liquid droplets in the present study was found to be opposite to that of conventional ratchet microstructures regardless of surface temperature and structure size. The mechanism that is widely used to describe the motion of a Leidenfrost droplet on a ratchet surface is known as the viscous mechanism (Dupeux et al. 2011). This mechanism is based on the preferential direction of vapor flow underneath the droplet. This vapor flow drags the droplet in a direction opposite to the tilt of the ratchet as a result of viscous stresses. Our experimental results could not be, however, explained by this mechanism; hence, a new mechanism for a self-propelled droplet on asymmetric three-dimensional self-organized microstructured surfaces is proposed. A schematic drawing of the proposed mechanism is shown in Fig. 8. It has been shown experimentally (Dupeux et al. 2011) that the vapor from an evaporating liquid droplet flows in the direction of descending slope on the teeth of a ratchet (*x*-direction on Fig. 8-top). When the flow encounters the next ratchet, it is redirected 90° (*y*-direction on Fig. 8 top) and flows down the ratchet channels (Dupeux et al. 2011). Flow in the *y*-direction is unobstructed; therefore, there exists only a net force in the *x*-direction, which results in the motion of the droplet with the same direction as the vapor flow (Fig. 8 top). This also means that each of the ratchet segments is cellular in the *x*-direction and develops a similar, yet independent, flow and force.

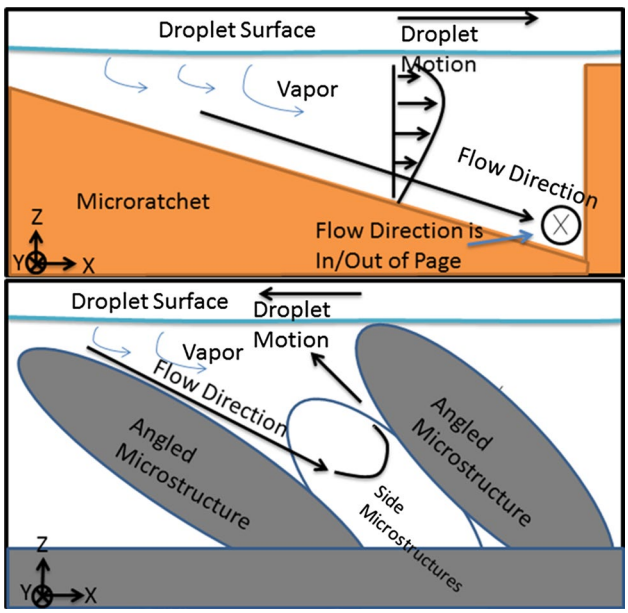

Fig. 8 *Top*—schematic describing mechanism governing droplet motion on conventional ratchet microstructures. *Bottom*—schematic describing proposed mechanism governing droplet motion on angled FLSP microstructures

In principle, the physics of the viscous mechanism must also apply to the angled FLSP microstructures. However, as shown by the present experimental results, this theory does not fully describe why droplet motion on the angled FLSP samples is in the opposite direction of that on ratchet structures. If the angled FLSP microstructures were reduced to their simplest form, they would be similar to the ratchet microstructures, however, with one critical difference. Because the angled FLSP microstructures are three dimensional and self-organized, they result in no channel in the *y*-direction, unlike with the ratchet structures. This difference is the key to understanding why the direction of droplet motion is different between the two structures. When vapor is released from a droplet on angled FLSP microstructures, the released vapor initially follows a very similar profile as in the case of the ratchet structures. However, because with the angled FLSP microstructures, there is no continuous path in the *y*-direction, and the vapor flowing into the spacing surrounded by neighboring microstructures is forced to be redirected nearly 180° (see Fig. 8 bottom). The redirected vapor drags the droplet with it through the viscous forces and causes the droplet to move in the opposite direction than that reported with the ratchet microstructures. Unlike the ratchet structures, the angled FLSP microstructures provide x- and y-direction cellular spacings, each independently generating a net force on the liquid droplet. Given the three-dimensional and self-organized nature of the angled FLSP microstructures, it is possible to have local vapor flows opposite to the droplet motion; however, they do not derail it from its main trajectory.

5 Conclusions

It has been shown in the present work that angled microstructures created through the use of FLSP can be used to effectively propel liquid droplets in the Leidenfrost state across a heated surface. Angled FLSP microstructures consist of mound-like structures with a rounded top that lean at a specific angle. These structures can be created at nearly any inclination angle. For this study, two surfaces were created with angles of 45° and 10° with respect to the surface normal. Self-propelled droplet motion experiments resulted in maximum velocities of 13.5 and 19.2 cm/s for the 10° and 45° samples, respectively. These maximum velocities occurred at temperatures well below the corresponding Leidenfrost temperatures of the surfaces. The high velocities at temperatures below the Leidenfrost temperatures of the surfaces are due to intermittent contacts of the liquid droplet with the surface microstructures. When this occurs, more energy is transferred to the droplet and vapor is violently ejected from the droplet. This vapor is preferentially directed by the microstructures into one general direction. In comparison with conventional

ratchet structures, the angled FLSP microstructures result in droplet motion in the opposite direction. This change in the direction of the droplet motion is due to the three-dimensional self-organized nature of the angled FLSP microstructures which leads to a redirection of the vapor flow. The viscous stress forces of the redirected vapor flow move the droplet in a direction opposite to that of the conventional ratchet structures that have been previously reported in the literature.

Acknowledgments This work has been supported by a grant through the Nebraska Center for Energy Sciences Research (NCESR) with funds provided by Nebraska Public Power District (NPPD) to the University of Nebraska–Lincoln (UNL) No. 4200000844, a NASA EPSCoR Grant # NNX13AB17A and by funds from the Department of Mechanical and Materials Engineering and the College of Engineering at UNL, awarded to SN.

References

Agapov RL, Boreyko JB, Briggs DP et al (2014) Length scale of Leidenfrost ratchet switches droplet directionality. Nanoscale. doi:10.1039/c4nr02362e

Bradfield W (1966) Liquid–solid contact in stable film boiling. Ind Eng Chem Fundam 5:200–204

Brochard F (1989) Motions of droplets on solid surfaces induced by chemical or thermal gradients. Langmuir 5:432–438

Brzoska J, Brochard-Wyart F, Rondelez F (1993) Motions of droplets on hydrophobic model surfaces induced by thermal gradients. Langmuir 9:2220–2224

Chaudhury M, Whitesides G (1992) How to make water run uphill. Science 256:1539–1541

Darhuber AA, Valentino JP, Davis JM et al (2003) Microfluidic actuation by modulation of surface stresses. Appl Phys Lett 82:657. doi:10.1063/1.1537512

Dos Santos F, Ondarcuhu T (1995) Free-running droplets. Phys Rev Lett 75:2972

Dupeux G, Le Merrer M, Lagubeau G et al (2011) Viscous mechanism for Leidenfrost propulsion on a ratchet. EPL Europhys Lett 96:58001. doi:10.1209/0295-5075/96/58001

Grounds A, Still R, Takashina K (2012) Enhanced droplet control by transition boiling. Sci Rep 2:720. doi:10.1038/srep00720

Hashmi A, Xu Y, Coder B et al (2012) Leidenfrost levitation: beyond droplets. Sci Rep 2:797. doi:10.1038/srep00797

Hwang TY, Guo C (2011) Polarization and angular effects of femtosecond laser-induced nanostructure-covered large scale waves on metals. J Appl Phys. doi:10.1063/1.3646330

John K, Bär M, Thiele U (2005) Self-propelled running droplets on solid substrates driven by chemical reactions. Eur Phys J E Soft Matter Biol Phys 18:183–199. doi:10.1140/epje/i2005-10039-1

Kim H, Truong B, Buongiorno J, Hu L-W (2011) On the effect of surface roughness height, wettability, and nanoporosity on Leidenfrost phenomena. Appl Phys Lett 98:083121. doi:10.1063/1.3560060

Kruse C, Anderson T, Wilson C et al (2013) Extraordinary shifts of the Leidenfrost temperature from multiscale micro/nanostructured surfaces. Langmuir 29:9798–9806. doi:10.1021/la401936w

Lagubeau G, Le Merrer M, Clanet C, Quéré D (2011) Leidenfrost on a ratchet. Nat Phys 7:395–398. doi:10.1038/nphys1925

Linke H, Alemán B, Melling L et al (2006) Self-propelled Leidenfrost droplets. Phys Rev Lett 96:2–5. doi:10.1103/PhysRevLett.96.154502

Marin AG, del Cerro DA (2012) Capillary droplets on Leidenfrost micro-ratchets. Phys Fluids 24:122001

Nayak BK, Gupta MC, Kolasinski KW (2007) Formation of nano-textured conical microstructures in titanium metal surface by femtosecond laser irradiation. Appl Phys A 90:399–402. doi:10.1007/s00339-007-4349-2

Ok JT, Lopez-Oña E, Nikitopoulos DE et al (2010) Propulsion of droplets on micro- and sub-micron ratchet surfaces in the Leidenfrost temperature regime. Microfluid Nanofluidics 10:1045–1054. doi:10.1007/s10404-010-0733-x

Piroird K, Clanet C, Quéré D (2012) Magnetic control of Leidenfrost drops. Phys Rev E 85:10–13. doi:10.1103/PhysRevE.85.056311

Tsibidis GD, Stratakis E, Loukakos PA, Fotakis C (2013) Controlled ultrashort-pulse laser-induced ripple formation on semiconductors. Appl Phys A 114:57–68

Vorobyev AY, Guo C (2013) Direct femtosecond laser surface nano/microstructuring and its applications. Laser Photonics Rev 7:385–407. doi:10.1002/lpor.201200017

Zuhlke CA, Anderson TP, Alexander DR (2013a) Formation of multiscale surface structures on nickel via above surface growth and below surface growth mechanisms using femtosecond laser pulses. Opt Express 21:8460–8473

Zuhlke CA, Anderson TP, Alexander DR (2013b) Comparison of the structural and chemical composition of two unique micro/nanostructures produced by femtosecond laser interactions on nickel. Appl Phys Lett 103:121603. doi:10.1063/1.4821452